Cosmic-Ray Muon Intensity Deep Underground versus Depth*

B. S. MEYER† AND J. P. F. SELLSCHOP
University of the Witwatersrand, Johannesburg, Republic of South Africa

AND

M. F. CROUCH
Case Western Reserve University, Cleveland, Ohio 44106

AND

W. R. KROPP, H. W. SOBEL, H. S. GURR, J. LATHROP, AND F. REINES
University of California, Irvine, California 92664

(Received 15 December 1969)

Cosmic-ray muons produced in the earth's atmosphere were measured at a depth of 8.71×10^5 g cm^{-2} with a large-area (170 m^2) liquid-scintillation-detector hodoscope. These data taken together with those of other workers lead to an improved muon vertical-depth intensity curve, $I_v(h)=a_\mu e^{-h/\lambda}$, where $I_v(h)=$vertical intensity, $a_\mu=(1.04_{-0.13}{}^{+0.21})\times10^{-6}$ cm^{-2} sec^{-1} sr^{-1}, $\lambda=(8.04_{-0.39}{}^{+0.35})\times10^4$ g cm^{-2}, and $h=$depth in g cm^{-2}. A comparison of these results with those expected from the sea-level muon spectra via an improved calculation may indicate the need for an increased energy loss, probably via the photonuclear interaction as suggested by Keuffel *et al.* The results are not inconsistent with the presence of the X process of Keuffel *et al.*

I. INTRODUCTION

A DETECTOR, designed primarily to record muons produced by the interactions of high-energy atmospheric neutrinos, was constructed at a depth of 8.71×10^5 g cm^{-2} in the East Rand Proprietary Mine (ERPM) near Johannesburg.[1] The detector also recorded a number of muons of atmospheric origin which penetrated the rock overburden, providing the muon intensity at a greater depth than was hitherto available. The present paper concerns itself with these atmospheric muons, and uses our data to improve knowledge of the vertical intensity variation with depth.

An improved numerical method for calculating the range fluctuations of muons in rock is developed. Using this technique and the existing formulas for muon energy loss, the energy spectrum of muons in the atmosphere was deduced from the curve of intensity versus depth. In order to obtain agreement with the energy spectrum deduced from extensive air showers, an increase in energy loss over that generally accepted is indicated.

A comparison of the vertical intensity with intensities measured at inclined angles does not exclude production of muons directly or via an extremely short-lived progenitor (X process) of the magnitude proposed by Keuffel *et al.*[2]

II. APPARATUS

The detector array (Fig. 1) was subdivided into nine bays, each consisting of six elements. The elements (Fig. 2) were Lucite tanks filled with liquid scintillator.[3]

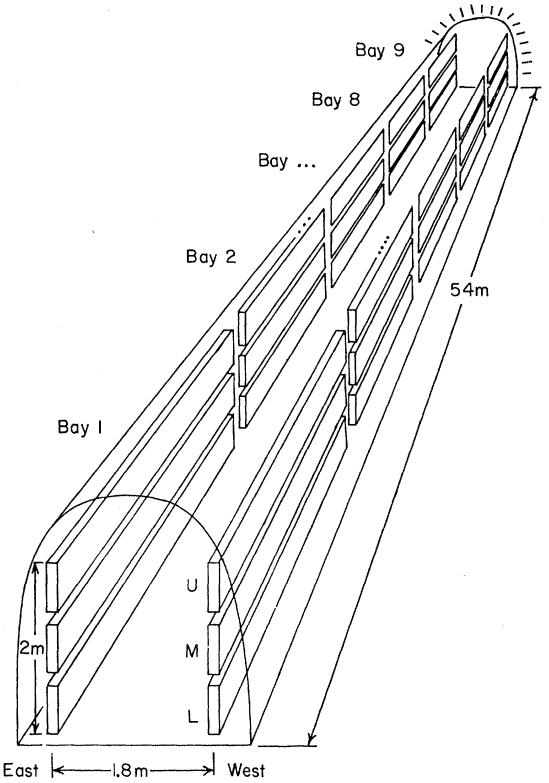

FIG. 1. Sketch of the detector array. Approximate dimensions are given to indicate the large size of the array.

* Work performed under the auspices of the U. S. Atomic Energy Commission.

† Present address: Weizmann Institute, Rehovoth, Israel.

[1] A full paper discussing the neutrino aspect of this experiment is in preparation. A brief preliminary account appeared in 1965 [F. Reines, M. F. Crouch, T. L. Jenkins, W. R. Kropp, H. S. Gurr, G. R. Smith, J. P. F. Sellschop, and B. Meyer, Phys. Rev. Letters **15**, 429 (1965)].

[2] J. W. Keuffel, J. L. Osborne, G. L. Bolingbroke, G. W. Mason, M. O. Larson, G. H. Lowe, J. H. Parker, R. O. Stenerson, and H. E. Bergeson, in Proceedings of the Eleventh International Conference on Cosmic Rays, Budapest, Hungary, 1969 (unpublished).

[3] M. F. Crouch, H. S. Gurr, A. A. Hruschka, T. L. Jenkins, W. R. Kropp, F. Reines, and H. W. Sobel, IEEE Trans. Nucl. Sci. **NS-13**, 424 (1966).

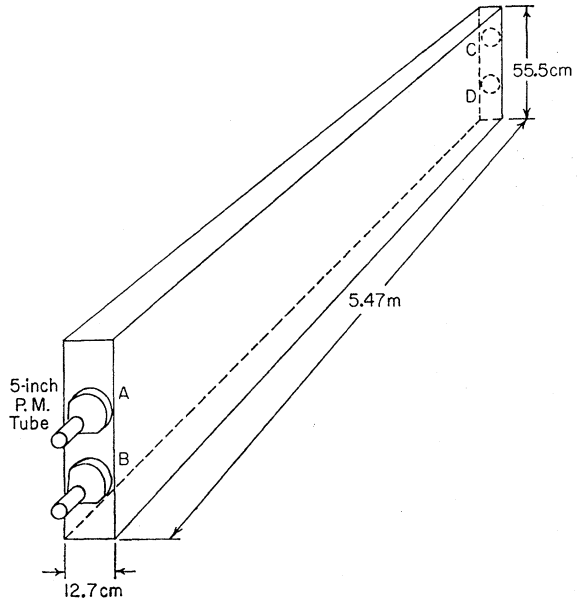

FIG. 2. Sketch of a detector element used in bays 1–6. The elements used in bays 7–9 differed by having a 38-cm nonscintillating region at each end.

The scintillating volume had dimensions $5.55\times0.56\times0.127$ m. Four photomultiplier tubes, designated A, B, C, and D, viewed each element. The outputs from all tubes fed an arrangement of delay lines, fan-outs, and fan-ins, which generated coded analog patterns identifying the elements involved and giving the four pulse heights from each of these elements. The interpretation of the pattern was ambiguous only for those rare events which involved more than one bay on the same side of the array. Sample oscilloscope patterns are shown in Fig. 3. Details of the detectors and the electronics have been published elsewhere.[3,4]

Pulses from the detector were recorded whenever they included A, B, C, and D signals from the same side (i.e., east or west) and were coincident within ~1 μsec. Accidental triggers were further reduced by the requirement that all four pulses originate either in bays 1–6 or in bays 7–9. A muon passing through a single element met these trigger requirements.

III. CALIBRATION

The overwhelming majority of muons reaching our detector had sufficient energy to penetrate the detector elements. The amount of energy which they deposited in the process varied, depending on the length of path in the scintillator, on Landau fluctuations, and, to a lesser extent, on the muon energy. A horizontally moving muon deposited about 20 MeV, while one moving vertically deposited about 90 MeV. The fraction of the scintillation light which reached the photomultiplier tubes depended on the position of the scintillation within the element. These effects were studied with identical elements at the surface of the earth, by selecting cosmic-ray muons with known paths using two small guide detectors. It was found in this way that the ratio of pulse heights $(A+B)/(C+D)$ gave the position of the scintillation along the active length of the element to within ±0.15 m irrespective of the path length in the scintillator. The error in estimating the path length, or equivalently (in the approximate sense outlined above) the energy deposited in the scintillator, is found to be roughly constant for all muon trajectories. This means that events in our detector having nearly horizontal paths could have errors of the order of $\pm50\%$ in their apparent energy depositions, while events which were vertical would have errors of the order of $\pm20\%$.

At our depth, the flux of muons through the detector was very small and could not be used directly to calibrate the detection system. It was therefore necessary to use secondary calibration techniques to relate the response to muons as measured at the surface station. The most practical method was found to be the production of fluorescence radiation in the scintillator by a

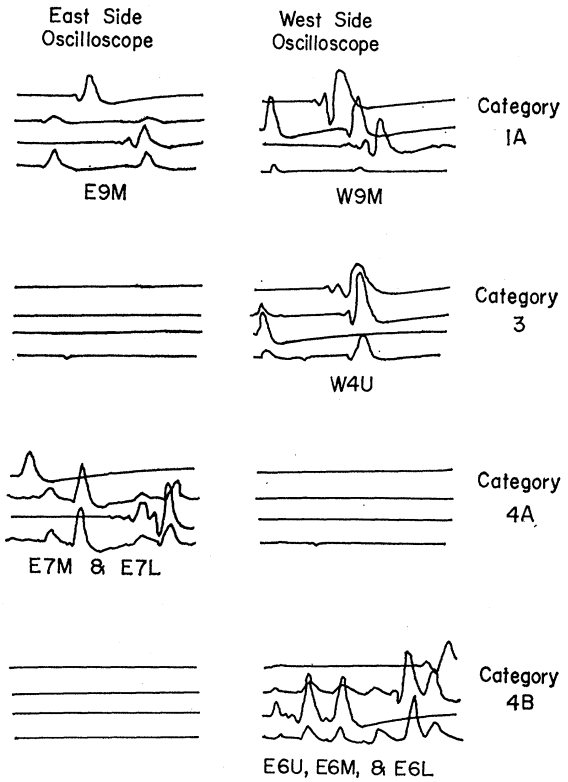

FIG. 3. Typical oscilloscope records of events involving categories 1A, 3, 4A, and 4B. Detector elements are designated by side of array (east or west), bay number, and position on a given side (upper, middle, or lower).

[4] M. F. Crouch, H. S. Gurr, W. R. Kropp, B. Meyer, and F. Reines, IEEE Trans. Nucl. Sci. **NS-13**, 432 (1966). More details on the experiment and a preliminary analysis of results may be found in B. S. Meyer, Ph.D. thesis, University of the Witwatersrand, 1969 (unpublished).

TABLE I. Definitions and populations of the various data categories. Based on data collected between 28 June 1965 and 23 August 1967.

Category	Number of detector elements involved	Locations of signals in the array	Observed populations Bays 1–6	Bays 7–9
1A	2	1 east side, 1 west side	18	7
1B	3	2 on one side, 1 on the other	4	0
2A	>3	Both sides	7	2
2B	≥2	Not classifiable into other categories	1	2
3	1	Anywhere in array	166	72
4A	2	Adjacent elements, one above the other	36	14
4B	3	Adjacent elements, one above the other	24	5
5	1	Two signals a few μsec apart	3	0

pulse of ultraviolet light.[5] The energy equivalent of the light pulser was determined by comparing pulses generated by it with those resulting from cosmic-ray muons moving along a known trajectory.

Intercomparison of the various secondary calibration techniques employing radioactive sources showed the error in the absolute energy calibration to be less than ±10%. The inherent stability of the system together with frequent calibrations (approximately one per month) enabled us to maintain the over-all gain to within ±10% during the several-year course of the experiment.

IV. BACKGROUNDS

A. Natural Background

A cosmic-ray muon measurement performed at such great depths is unique in that neutrino-induced muons are a major source of background (see Sec. VI).

A second possible contribution to the background may arise from high-energy γ rays which produce single-element events. These may be produced in the spontaneous fission of U^{238} found in the rock surrounding our detector. A conservative estimate indicates the contribution from this source to be negligible.[6]

Low-energy γ rays from natural radioactive decay are another form of background. The threshold discriminators eliminated all single γ-ray events with energies less than 8 MeV deposited at the center of an element. Nevertheless, the chance coincidence of two low-energy γ rays, one at an A, B end and one at a C, D end, could trigger the detector array. The discriminators were triggered in this case because of the proximity of the low-energy interactions to the phototubes; the steeply rising response function of the detector elements (Fig. 4) gave such a chance coincidence the appearance of a higher-energy single interaction. In most of these cases two different elements were involved, and such events could therefore be readily eliminated by an examination of the film record. In the rare case where both low-energy γ rays were confined to a single element, the resolving time of the oscilloscope record (0.2 μsec) was adequate to reduce the residual rate to a negligible number (<1 per yr).

B. Artificial Background

The low rate of events due to cosmic rays plus neutrinos, about one in 2 days, required that the system be capable of discriminating against electrical noise and other instrumental effects.

The electric power was isolated from outside interference by using a motor-generator set followed by a low-pass filtering network. Spurious effects occasionally observed were traceable to sources inside the system, e.g., bad electrical contacts. However, such effects were easily recognizable from the waveforms of the pulses displayed on the oscilloscopes. It was also found that seismic activity in the mine, due mainly to blasting, could simulate single-tank events. Accordingly, a set of geophones was installed to permit rejection of triggers which occurred in coincidence with such activity.

V. DATA

The experiment has produced a rich assortment of data which, because of the detector geometry, divides conveniently into a number of categories. The definitions and populations of these categories are given in Table I.

For the present analysis, we are interested in the intensity and the angular distribution of the atmospheric muons. These must be separated from the

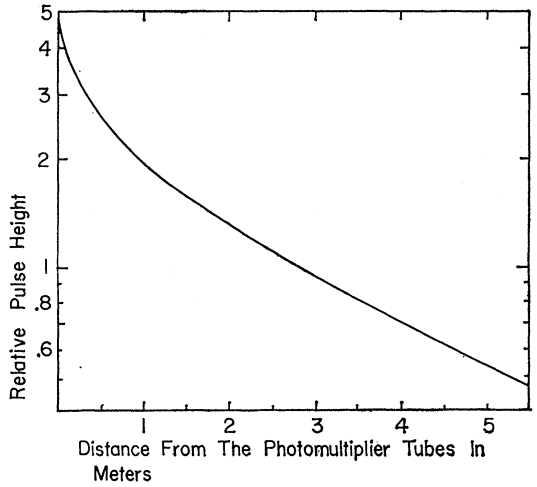

FIG. 4. Response function of an element from bays 1–6.

[5] H. S. Gurr, Ph.D. thesis, Case Institute of Technology, 1966 (unpublished).

[6] An independent experiment performed by H. W. Sobel *et al.* (unpublished) at our site observed γ rays up to 20 MeV from a U^{238} source. Background spectra from this detector were used to predict the rate due to high-energy γ rays associated with the natural abundance of uranium in our rock surroundings.

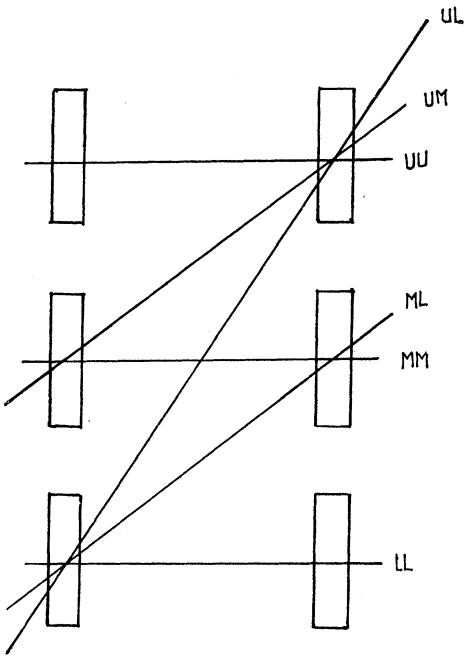

FIG. 5. Muon trajectories representing the three subclasses of category 1A.

muons which are produced in the rock by neutrinos. The key to this separation is the great difference in the angular distributions: The atmospheric muons are sharply peaked about the vertical, whereas the neutrino-produced muons favor the horizontal direction. Accordingly, we further sort the data into the following seven classes, where each class represents a particular range of zenith angles: (1) 1UU: type-1A or 1B events in UU or MM or LL elements; (2) 1UM: type-1A or 1B events in UM or ML elements; (3) 1UL: type-1A or 1B events in UL elements; (4) 3UL: type-3 events in U or L elements; (5) 3M: type-3 events in M elements; (6) 4A: type-4A events; (7) 4B: type-4B events. We use the codes U, M, and L to represent upper, middle, and lower elements, respectively. Figures 5–7 show typical muon trajectories which give rise to events in these classes.

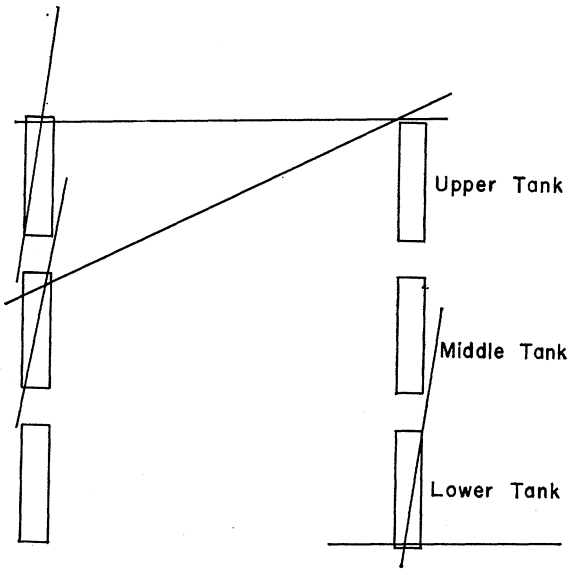

FIG. 6. Range of zenith angles accessible to upper, middle, and lower elements for category-3 events.

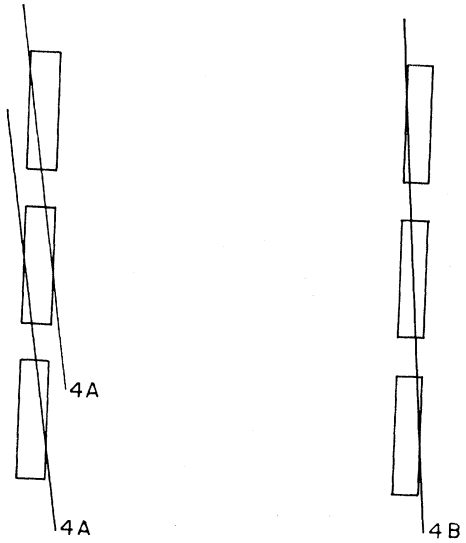

FIG. 7. Muon trajectories which give rise to events of type 4A and 4B.

The 1B events are multiparticle, most likely consisting of a muon and secondaries. The energies deposited in each of the three elements involved indicate the most likely muon trajectory. The 1B events have been placed in class 1, 2, or 3 on this basis.

The geometry of the detector also rules out a single-particle interpretation of category 2A and 2B events. It is most likely that these are the result of electromagnetic showers produced by muons in the rock above the detector. Since the width of the detector element (0.13 m) is small compared with the separation between the east and the west sides of the array (1.8 m), we conclude it to be unlikely that the initiating muon itself passed through an element. In addition, we see from Table I that the number of events in these classes is so small that the errors which result from ignoring them are negligible.

Category-5 events have been interpreted as low-energy, neutrino-induced muons which stop in a detector element and then decay. This interpretation will be discussed in the forthcoming paper on atmospheric neutrinos.[1]

Since bays 1–6 and 7–9 are geometrically different (albeit slightly, see Table II), we have treated them as independent systems. We thus have 14 classes of events, seven for each group of bays. The population and sensitive time of each class are given in Table III.

TABLE II. Dimensions of the detector elements and their spacing in the array. Directions are defined in Fig. 1.

	Bays 1–6 (m)	Bays 7–9 (m)
Length	5.47	4.71
North-South gap	0.59	1.36
Thickness	0.127	0.127
East-West gap	1.65	1.70
Height	0.555	0.555
Vertical gap	0.150	0.171

VI. VERTICAL INTENSITY VERSUS DEPTH

As discussed in Sec. VII, our experiment, performed at a depth of 8.71×10^5 g cm^{-2} of rock ($Z^2/A=5.53$; $Z/A=0.499$; $\rho=2.71$ g cm^{-3}), gives the intensity with an accuracy of about $\pm12\%$. In deriving the curve of vertical intensity versus depth for depths $\geq4\times10^5$ g cm^{-2}, we limited ourselves to data from experiments[7–10] of similar accuracy (i.e., better than $\sim30\%$). These are listed in Table IV.

A knowledge of the angular distribution of the atmospheric muons is necessary to determine the vertical intensity at a given detector. Unless directly measured, this distribution must be determined from the slope of the vertical-intensity–versus–depth curve, which, in turn, is found from the intensities measured with our detector and those of other workers; a process of iteration is required.

A. Angular Distributions

Calculations of the angular dependence of neutrino-induced muons indicate that the ratio of horizontal to vertical fluxes of these muons is $\lesssim3$.[11] We take this ratio as an upper limit and connect the two points by a smooth function

$$j_\nu(\theta)=1-\tfrac{2}{3}\cos^2\theta. \quad (1)$$

A lower limit for this ratio is unity, corresponding to an isotropic flux. Our conclusions are found to be relatively insensitive to the choice of an angular distribution between these two extremes.

Menon *et al.*[12] have used the experimental depth-intensity curve to arrive at an analytic form for the angular distribution of the atmospheric muons. The intensity at a vertical depth h ($\geq4\times10^5$ g cm^{-2}), has the form

$$I_\mu(h,\theta=0)=I_v=a_\mu e^{-h/\lambda}. \quad (2)$$

If we assume that the surface of the earth above the detector is a horizontal plane,[13] the muons moving at an angle θ will be attenuated by a factor $e^{-h\sec\theta/\lambda}$ upon penetrating to a vertical depth h. If the muons are produced by the decay of π and K mesons, the angular distribution of muons will be proportional to $\sec\theta$ at the surface.[14] Accordingly, the intensity at a vertical depth h and angle θ underground will be

$$I_\mu(h,\theta)=a_\mu\sec\theta e^{-h\sec\theta/\lambda}. \quad (3)$$

As already mentioned, Keuffel and co-workers[2,15] have suggested that a small fraction of the atmospheric muons may be produced directly or by means of a short-lived intermediary (X process). If this were the case, these muons would have the same spectral index as the primary spectrum and an isotropic angular distribution in the atmosphere. The relatively slow falloff with energy of this portion of the total muon flux increases its importance at large energies (or depths). As an

TABLE III. Number of events and sensitive times, based on data collected between 28 June 1965 and 23 August 1967.

Bays	Class	Sensitive time (h)	Number of events
1–6	1UU	14475	11
	1UM	14475	8
	1UL	14475	3
	3UL	14377	113
	3M	14377	53
	4A	14475	36
	4B	14475	24
7–9	1UU	12083	3
	1UM	12083	3
	1UL	12083	1
	3UL	12055	50
	3M	12055	22
	4A	12083	14
	4B	12083	5

TABLE IV. Vertical intensities measured by other workers.

Actual depth (10^5 g cm^{-2})	Equivalent depth in standard rock (10^5 g cm^{-2})	Vertical intensity (cm^{-2} sec^{-1} sr^{-1})
Achar *et al.*, 4.10	4.40	$(4.63\pm0.57)\times10^{-9}$
Castagnoli *et al.*, 4.11	3.97	$(1.00\pm0.23)\times10^{-8}$
Miyake *et al.*, 4.28	4.61	$(3.24\pm0.35)\times10^{-9}$
6.38	6.97	$(1.92\pm0.47)\times10^{-10}$
Menon *et al.*, 7.00	7.67	$(1.05\pm0.34)\times10^{-10}$

[7] S. Miyake, V. S. Narasimham, and P. V. Ramana Murthy, Nuovo Cimento **32**, 1905 (1964).
[8] C. Castagnoli, A. DeMarco, A. Longhetto, and P. Penengo, Nuovo Cimento **35**, 969 (1965).
[9] C. V. Achar, V. S. Narasimham, P. V. Ramana Murthy, D. R. Creed, J. B. M. Pattison, and A. W. Wolfendale, Proc. Phys. Soc. (London) **86**, 1305 (1965).
[10] M. G. K. Menon, S. Naranan, V. S. Narsimham, K. Hinotani, N. Ito, S. Miyake, D. R. Creed, J. L. Osborne, and A. W. Wolfendale, Can. J. Phys. **46**, S344 (1968).
[11] R. Cowsik, Yash Pal, T. N. Rengarajan, and S. N. Tandon, in *Proceedings of the International Conference on Cosmic Rays, Jaipur, India, 1963* (Commercial Printing Press, Ltd., Bombay, India, 1964–5), Vol. 6, p. 211.
[12] M. G. K. Menon, S. Naranan, V. S. Narasimham, K. Hinotani, N. Ito, S. Miyake, D. R. Creed, J. L. Osborne, J. B. M. Pattison, and A. W. Wolfendale, Proc. Phys. Soc. (London) **90**, 646 (1967).
[13] This is an excellent approximation because the rapid falloff of the atmospheric muon spectrum with energy causes the angular distribution at great depths to be sharply peaked to the vertical.
[14] The $\sec\theta$ dependence is an approximation, valid only for small zenith angles and large energies. These conditions are clearly satisfied for cosmic-ray muons penetrating to great depths.
[15] H. E. Bergeson, J. W. Keuffel, M. O. Larson, E. R. Martin, and G. W. Mason, Phys. Rev. Letters **19**, 1487 (1967).

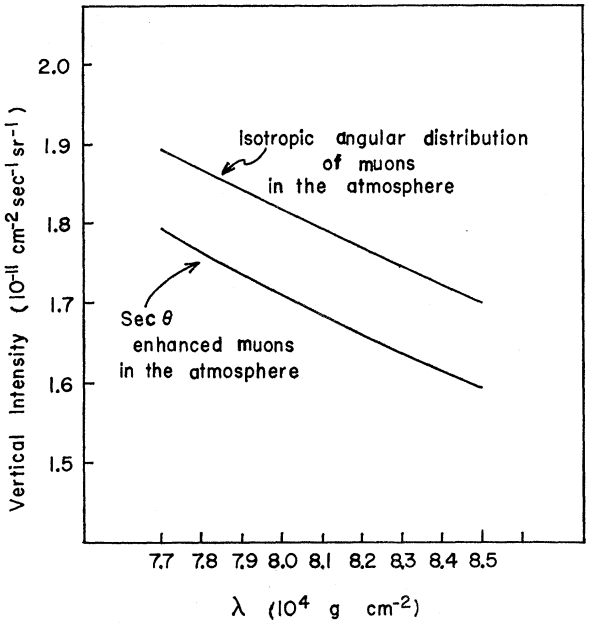

FIG. 8. Vertical intensity of atmospheric muons at our site expressed as a function of the parameter λ, for isotropic and secθ enhanced muons in the atmosphere and an isotropic angular distribution of neutrino-induced muons.

extreme test of the sensitivity of our vertical intensity to the form of the angular distribution, we have assumed that all of the muons capable of penetrating to our depth are isotropic as they enter the earth. In this case,

$$I_\mu(h,\theta)=a_\mu e^{-h\ \sec\theta/\lambda}. \tag{4}$$

B. Intensity at Our Site

To find the intensity of atmospheric muons at our detector, we need to know the fraction and angular distribution of events due to neutrino-induced muons. We have used the following method to calculate the contributions of these two components to the total number of counts, C. Using the subscript i to denote one of the 14 classes of events, where t_i is the sensitive time for class i, $dA_i/d\theta$ is the relevant differential aperture (see Appendix A) and $I(h,\theta)$ is the sum of the intensities of atmospheric and neutrino-induced muons, we get

$$C_i=t_i\int_0^\pi I(h,\theta)\frac{dA_i}{d\theta}d\theta. \tag{5}$$

The likelihood L of the observed numbers of events, N_i, if the expected numbers are C_i, is

$$L=\prod_{i=1}^{14} e^{-C_i}\frac{C_i^{N_i}}{N_i!}. \tag{6}$$

This follows, since each count rate obeys the Poisson distribution. $I(h,\theta)$ can be expressed as

$$I(h,\theta)=a_\mu j_\mu(\theta)+a_\nu j_\nu(\theta), \tag{7}$$

where $j_\mu(\theta)$ and $j_\nu(\theta)$ are the angular distributions and a_μ and a_ν are parameters which we fitted to the data of our experiment. The subscript μ refers to that part of the intensity due to atmospheric muons and ν to that part due to neutrino-induced muons.

The best estimates of the parameters a_μ and a_ν are those which maximize L. The vertical intensity at our detector site is then found by subsitution of a_μ into Eq. (2).

In order to simplify the iterative process required, we have plotted the vertical intensity of atmospheric muons at our detector site as a function of the parameter λ for the four combinations of angular distributions. These are given in Figs. 8 and 9.

C. Intensities Measured by Other Workers

In the experiments of Achar *et al.*[9] and of Menon *et al.*[10] the angular distribution was measured directly. We, therefore, use their vertical intensities without correction.

For the experiments of Castagnoli *et al.*[8] and of Miyake *et al.*,[7] the angular distribution was determined from the variation of the vertical intensity with depth. These authors have calculated the effective apertures of their detectors as a function of the parameter n, which appears in the following alternative empirical expression for the intensity of muons with zenith angle θ:

$$I_\mu(h,\theta)=a_\mu j_\mu(h,\theta)=I_v\cos^n\theta. \tag{8}$$

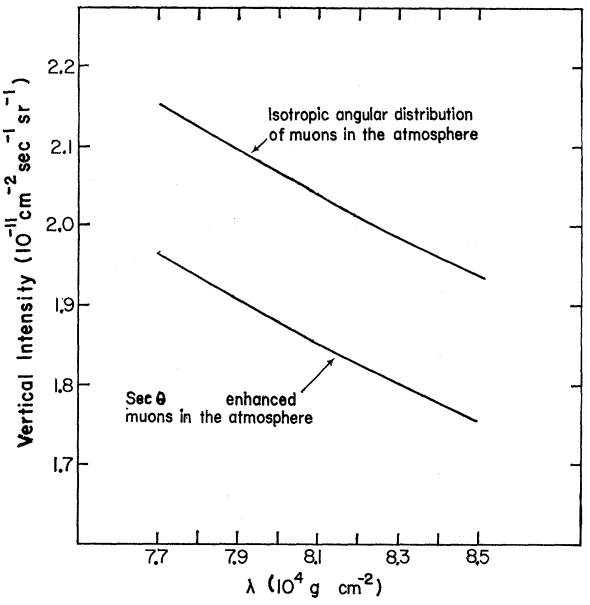

FIG. 9. Vertical intensity of atmospheric muons at our site expressed as a function of the parameter λ, for isotropic and secθ enhanced muons in the atmosphere and $j_\nu=1-0.67\cos^2\theta$.

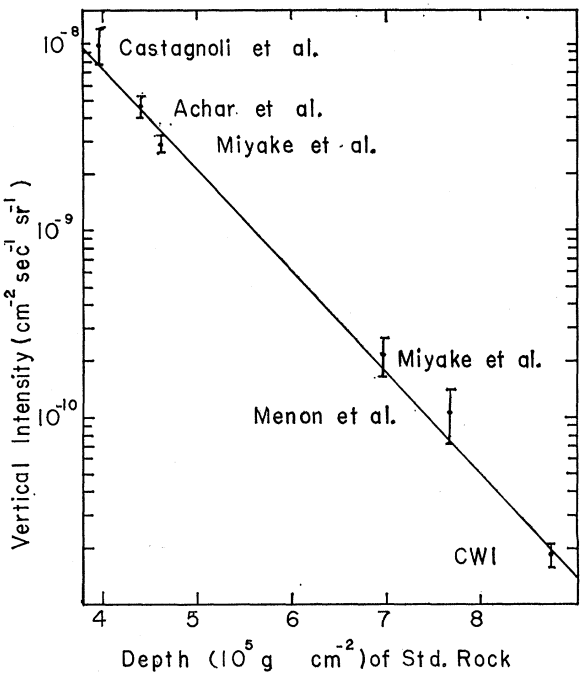

FIG. 10. Vertical intensity versus depth for muons in standard rock, assuming secθ enhancement for muons in the atmosphere and $j_\nu = 1 - 0.67\cos^2\theta$.

If the muons in the atmosphere are enhanced by secθ, it follows from Eq. (3) that for small θ

$$n \simeq h/\lambda - 1. \tag{9}$$

If all of the muons are isotropic in the atmosphere, then Eq. (4) applies and it follows that

$$n \simeq h/\lambda. \tag{10}$$

As shown in Sec. IX, the additional information from our experiment enables us to determine λ to greater accuracy than was available to previous workers. Since λ is directly given by the angular distribution coefficient n [Eqs. (9) and (10)], we are able to perform a more accurate transformation of the measured intensities of other workers into vertical intensities.

D. Equivalent Depths in Standard Rock

We have used the formula given by Menon and Ramana Murthy[16] to find the equivalent depths in standard rock ($Z^2/A = 5.5$; $Z/A = 0.5$; $\rho = 2.65$ g cm^{-3}), h_0, of the various experimental sites

$$h_0 = (1/b_0)\ln[1 + (b_0/b)(e^{bh} - 1)]. \tag{11}$$

Here, h is the actual depth, h_0 is the equivalent depth, and b and b_0 are the energy-loss coefficients for actual and standard rock, respectively. The coefficient b is defined in Appendix B, where it is found that for a given value of the photonuclear cross section, and at energies larger than about 10^{12} eV, b is constant and can be written as the sum of two terms, one proportional to Z^2/A of the rock, and the other to the photonuclear cross section $\sigma_{h\nu}$ [Eq. (B7)].

[16] M. G. K. Menon and P. V. Ramana Murthy, *Progress in Elementary Particles and Cosmic Ray Physics* (North-Holland, Amsterdam, 1967), Vol. 9, p. 163.

TABLE V. Quantities deduced from the vertical-intensity–versus–depth curve, where the vertical intensity at depth h is $a_\mu e^{-h/\lambda}$.

Neutrino-induced muon angular distribution	Atmospheric muon angular distribution	λ (10^4 g cm^{-2})	a_μ (10^{-6} cm^{-2} sec^{-1} sr^{-1})
$1-0.67\cos^2\theta$	sec θ	$8.04_{-0.39}^{+0.35}$	$1.04_{-0.13}^{+0.21}$
$1-0.67\cos^2\theta$	Isotropic	$8.08_{-0.33}^{+0.29}$	$1.09_{-0.15}^{+0.18}$
Isotropic	sec θ	$7.93_{-0.37}^{+0.36}$	$1.13_{-0.17}^{+0.20}$
Isotropic	Isotropic	$7.96_{-0.37}^{+0.28}$	$1.18_{-0.14}^{+0.22}$

E. Determination of Experimental Depth-Intensity Curves

Using a first estimate of the parameter λ, e.g., 8.1×10^4 g cm^{-2} deduced by Menon *et al.*,[12] and a pair of angular distributions for the two classes of muons, we deduce the intensity of muons from our experiment and those of Miyake *et al.* and Castagnoli *et al.* Taking these corrected intensities and depths, we find the best straight line through the data points on a plot of log intensity versus depth, using a weighted least-squares method. The slope of this graph gives an improved value of the parameter λ which is used in a second

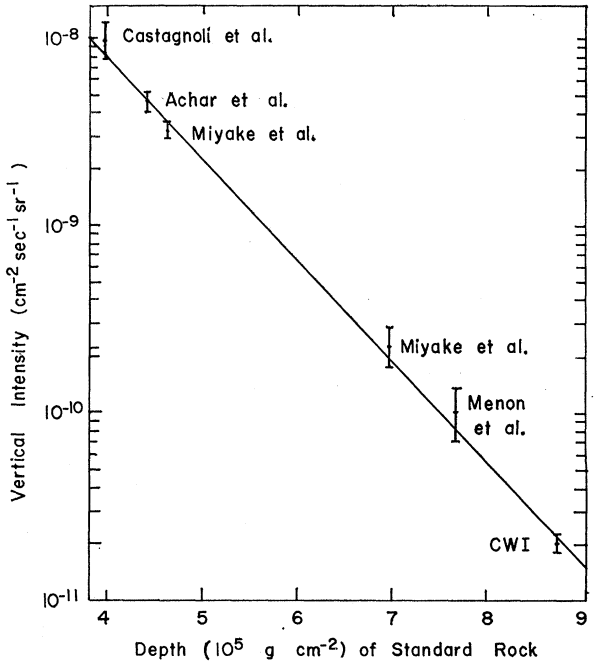

FIG. 11. Vertical intensity versus depth for muons in standard rock, assuming an isotropic distribution of muons in the atmosphere and $j_\nu = 1 - 0.67\cos^2\theta$.

TABLE VI. Corrected intensities and depths.

Atmospheric muon angular distribution		$\sec\theta$	Isotropic	$\sec\theta$	Isotropic
Neutrino-induced muon angular distribution		$1-0.67\cos^2\theta$	$1-0.67\cos^2\theta$	Isotropic	Isotropic
Author	Depth in standard rock (10^5 g cm^{-2})	Intensity (cm^{-2} sec^{-1} sr^{-1})	Intensity (cm^{-2} sec^{-1} sr^{-1})	Intensity (cm^{-2} sec^{-1} sr^{-1})	Intensity (cm^{-2} sec^{-1} sr^{-1})
Castagnoli *et al.*	3.97	$(9.74\pm2.24)\times10^{-9}$	$(9.85\pm2.27)\times10^{-9}$	$(9.73\pm2.24)\times10^{-9}$	$(9.86\pm2.27)\times10^{-9}$
Achar *et al.*	4.40	$(4.63\pm0.57)\times10^{-9}$	$(4.63\pm0.57)\times10^{-9}$	$(4.63\pm0.57)\times10^{-9}$	$(4.63\pm0.57)\times10^{-9}$
Miyake *et al.*	4.61	$(2.88\pm0.31)\times10^{-9}$	$(3.28\pm0.35)\times10^{-9}$	$(2.92\pm0.32)\times10^{-9}$	$(3.31\pm0.36)\times10^{-9}$
Miyake *et al.*	6.97	$(2.14\pm0.52)\times10^{-10}$	$(2.33\pm0.57)\times10^{-10}$	$(2.15\pm0.53)\times10^{-10}$	$(2.37\pm0.58)\times10^{-10}$
Menon *et al.*	7.67	$(1.05\pm0.34)\times10^{-10}$	$(1.05\pm0.34)\times10^{-10}$	$(1.05\pm0.34)\times10^{-10}$	$(1.05\pm0.34)\times10^{-10}$
CWI	8.74	$(1.87\pm0.23)\times10^{-11}$	$(2.04\pm0.25)\times10^{-11}$	$(1.73\pm0.21)\times10^{-11}$	$(1.83\pm0.23)\times10^{-11}$

TABLE VII. Maximum-likelihood parameters derived from the data of our experiment.

Case			Derived parameters	
Neutrino-induced muon angular distribution	Atmospheric muon angular distribution	λ (10^4 g cm^{-2})	a_μ ($\times10^{-6}$ cm^{-2} sec^{-1} sr^{-1})	a_ν ($\times10^{-13}$ cm^{-2} sec^{-1} sr^{-1})
$1-0.67\cos^2\theta$	$\sec\theta$	8.04	(1.11 ± 0.12)	(3.52 ± 0.66)
$1-0.67\cos^2\theta$	Isotropic	8.08	(1.15 ± 0.12)	(3.53 ± 0.66)
Isotropic	$\sec\theta$	7.93	(1.20 ± 0.16)	(3.30 ± 0.62)
Isotropic	Isotropic	7.96	(1.25 ± 0.15)	(3.30 ± 0.62)

cycle of iteration. This process of iteration converges in two or three cycles, giving the results listed in Tables V and VI. The errors quoted for the parameters λ and a_μ include a significant contribution due to our small depth uncertainty (see Sec. VII B).

A comparison of the various values of λ derived above shows that the results are not sensitive to the angular distribution of muons produced by neutrinos. Within the limiting cases we have chosen, λ changes by less than 1.5%.

The vertical intensities as calculated from the depth-intensity curves derived above show a 7% spread over the two extreme neutrino-muon angular distributions. The actual neutrino-muon angular distribution lies very close to the upper limit we have chosen. Therefore, in subsequent analyses, only the nonisotropic neutrino-muon angular distribution is used. For these two cases, we have plotted (Figs. 10 and 11) the corrected intensities and depths for the various experiments together with the derived depth-intensity curves.

Table VII gives the parameters for the atmospheric and neutrino muon fluxes derived from the maximum-likelihood calculation for the final iteration. The parameter a_ν will be more fully discussed in a forthcoming

TABLE VIII. Comparison of the observed data with the calculated number of events in each class. Calculations were performed with parameters derived from the experiment, using isotropic atmospheric muons and $j_\nu(\theta)=1-0.67\cos^2\theta$.

			Calculated number of events		
Bays	Class	Observed number of events	Atmospheric muons	Neutrinos	Total
1–6	1UU	11	0.0	9.1	9.1
	1UM	8	0.0	10.0	10.0
	1UL	3	0.1	3.0	3.1
	3UL	113	89.6	42.0	131.5
	3M	53	30.1	18.1	48.2
	4A	36	39.6	2.5	42.1
	4B	24	8.2	0.3	8.4
7–9	1UU	3	0.0	2.9	2.9
	1UM	3	0.0	3.1	3.1
	1UL	1	0.04	0.91	1.0
	3UL	50	33.3	16.7	50.0
	3M	22	11.6	7.4	18.9
	4A	14	13.6	0.9	14.5
	4B	5	3.2	0.1	3.3

TABLE IX. Comparison of the observed data with the calculated number of events in each class. Calculations were performed with parameters derived from the experiment, using $\sec\theta$ enhanced atmospheric muons and $j_\nu(\theta)=1-0.67\cos^2\theta$.

			Calculated number of events		
Bays	Class	Observed number of events	Atmospheric muons	Neutrinos	Total
1–6	1UU	11	0.0	9.1	9.1
	1UM	8	0.0	9.9	9.9
	1UL	3	0.2	3.0	3.2
	3UL	113	90.4	41.9	132.3
	3M	53	31.1	18.1	49.2
	4A	36	38.3	2.5	40.8
	4B	24	7.7	0.3	8.0
7–9	1UU	3	0.0	2.9	2.9
	1UM	3	0.0	3.1	3.1
	1UL	1	0.1	0.9	1.0
	3UL	50	33.6	16.6	50.2
	3M	22	11.9	7.3	19.3
	4A	14	13.2	0.9	14.0
	4B	5	3.0	0.1	3.1

paper on the neutrino portion of our signal. Tables VIII and IX give the predicted and observed populations of the various data categories.

VII. ERRORS IN DETERMINING OUR INTENSITY AND DEPTH

A. Errors in Intensity

There are several sources of error in the determination of the atmospheric muon intensity at our detector site. The largest, $\pm 11\%$, is a statistical error due to the fairly small number of data events. Simplifications in our aperture calculation introduce an error of $\pm 2.5\%$. Drifts in gain and calibration inaccuracies can cause an error in intensity of $\pm 5\%$. The resolution of our detector results in an intensity uncertainty of $\pm 0.75\%$. We conclude the resultant error in intensity arising from the above sources to be $\pm 12\%$.

We note that our maximum-likelihood calculation predicts fewer events for category 4B than are observed (Tables VIII and IX). We interpret this excess as due to muons accompanied by electron showers with a small lateral spread, the muon of the shower passing through the detector array. If this were not true, i.e., if all the muons missed the detector, then we have overestimated the intensity of atmospheric muons by about 8%. Category-2A events were interpreted as being due to showers with a large lateral spread, so that for these events, it is unlikely that the muon passed through the detector. If this interpretation is incorrect, i.e., if all the muons did pass through the detector, then we have underestimated the intensity of atmospheric muons by about 5%.

We have neglected any contribution to the category-3 rate arising from secondaries of those muons which miss our array. We are guided in this direction by the statistically equal number of upper, middle, and lower events in category 3. Because of the vertical nature of the cosmic rays and the geometry of our array, one would expect a larger number of lower events from this mechanism. The maximum overestimate of our vertical intensity from this assumption is about 6%.

B. Errors in Depth

The mining of gold at the ERPM is confined to a single layer of gold-bearing rock. Except for mine shafts which have been sunk through the overburden, and the outcrops of the various strata, there is no access to the strata which lie over the crosscut in which the detector array was located. The positions of the strata are therefore somewhat conjectural. On the other hand, the strata are very similar in chemical composition and density, so that very little error is to be expected in the calculations which were performed with the available data.

Individual strata were sampled in various accessible locations to determine the variation in density. In this way the error in density is determined to be $\pm 0.7\%$. The average density of our overburden varies as a function of zenith angle. By weighting each direction with the relative muon intensity appropriate to its zenith angle, we determine the error in density averaged over various directions to be $\pm 0.2\%$. The surface above our detector varies in elevation. A circle of radius 1900 m was studied giving each elevation a weight appropriate to the zenith angle it subtended at our detector. These contour errors were found to be $\pm 0.6\%$. The net error in depth from the above sources is $\pm 0.9\%$, and the depth of our detector is thus determined to be $(8.71 \pm 0.08) \times 10^5$ g cm^{-2}.

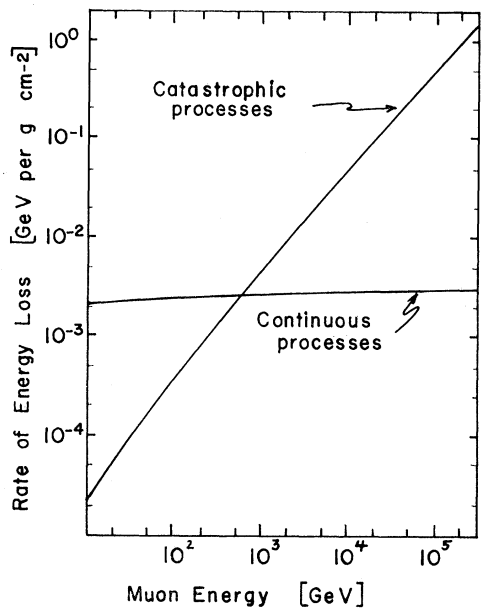

FIG. 12. Comparison between the rate of energy loss due to continuous processes and the average rate due to catastrophic processes for muons in ERPM rock.

VIII. DERIVATION OF SEA-LEVEL SPECTRUM

A. Range Fluctuations

If the energy loss of muons in matter were continuous, then muons of a given energy would have a unique range. Fluctuations in range arise from catastrophic processes, e.g., bremsstrahlung, and hence must be taken into account when the variation of the muon intensity with depth is calculated from the energy spectrum of the muons at the surface of the earth. Figure 12 shows that catastrophic interactions dominate the energy loss at energies greater than 600 GeV.

Several methods have been used in the past for the calculation of these range fluctuations.[16] We chose the numerical method of Raman Murthy[17] since it

[17] P. V. Ramana Murthy, Ph.D. thesis, University of Bombay, 1962 (unpublished).

enabled us to use the rather complex equations for the energy loss without introducing undue approximations, and also because it avoided the statistical errors inherent in the Monte Carlo method. Our contribution to Ramana Murthy's method lies in the choice of energy transfer for small fractional energy loss as described below.

The energy spectrum of the muons at a given depth is represented by the number of muons in each of a series of equally spaced energy bins. In calculating the energy distribution at each succeeding depth, the effects of the continuous and catastrophic energy-loss process are considered separately. It is convenient to deduce a curve which results in the absence of catastrophic processes. We call this curve, the solution of Eq. (B1), the energy-depth relationship for muons. In a given depth increment, the effect of the continuous energy loss on the boundaries of the energy bins is traced using this result (Fig. 13). In practice, the bin boundaries are held fixed and the muons are transferred from one bin to the next.

Since catastrophic processes cause muons to lose variable amounts of energy, the corresponding bin changes are variable and can be large. The probability that a muon at depth j (Fig. 14) in an energy bin with limits U_U and U_L goes, at depth $j+1$, into a bin with energy limits E_U and E_L is

$$\text{probability of transfer}=\int_{U_L}^{U_U}\int_{v=(U-E_U)/U}^{(U-E_L)/U} dh \times\varphi(U,v)dv\frac{dU}{U_U-U_L}. \quad (12)$$

Referring to Fig. 22, we see that the cross section $\varphi(U,v)$, due primarily to pair production at high energies and low fractional energy loss v per collision,

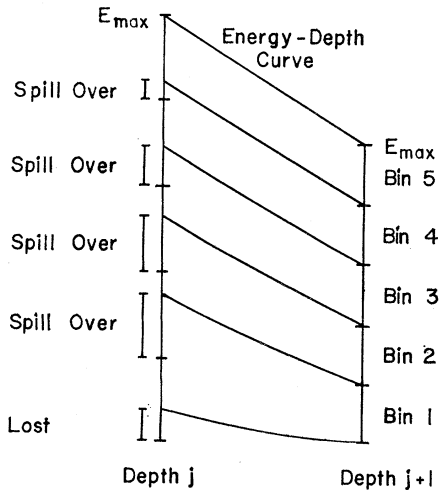

FIG. 13. Effect of a continuous energy-loss mechanism on the boundaries of our energy bins.

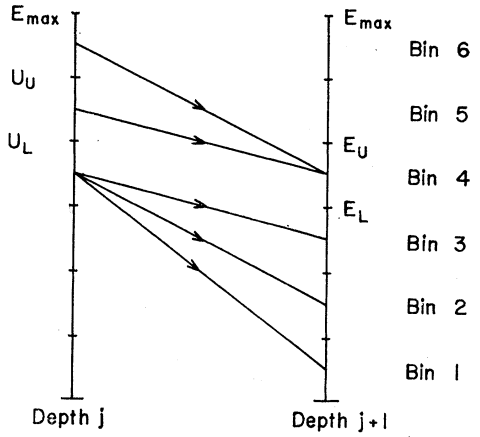

FIG. 14. Sample catastrophic energy transitions. In this illustration the symbols U_U, U_L, E_U, and E_L refer to the transition from bin 5 to bin 4.

varies rapidly with v. This behavior makes the integration of Eq. (12) inaccurate in the case of neighboring bins. Accordingly, we have devised the following method for calculating the number of muons transferred between such bins. Equation (12) is used to find the number of muons, n_{ij}, which are transferred from bin i to bin j, where $j=1, 2, \ldots, i-2$. Owing to their transfer to lower bins, these muons lose a combined energy given by

$$E_{\text{part}}=\sum_{j=1}^{i-2} n_{ij}(E_i-E_j), \quad (13)$$

where E_j is the median energy of the jth bin. Now, from the coefficient b of Eq. (B6), we calculate the total energy, which the muons in bin i should lose owing to the catastropic processes:

$$E_{\text{tot}}=b(E_i)E_i. \quad (14)$$

We then transfer $n_{i,i-1}$ muons to the bin $i-1$ so that the energy balance is correct, i.e.,

$$E_{\text{tot}}=E_{\text{part}}+n_{i,i-1}(E_i-E_{i-1}). \quad (15)$$

These calculations were preformed on the IBM 360/50 computer at the University of the Witwatersrand. The program was designed to find the probability $P(E,h)$ that muons with a given energy E at the surface would reach each of a series of depths h underground. A family of curves was generated for a series of initial energies. These curves are shown in Figs. 15 and 16 for two values of the photonuclear cross section.

B. Derivation of Parameters in Sea-Level Spectrum

In this section we derive a relationship between the spectral index γ in the power-law energy spectrum of muons in the atmosphere and the slope of the vertical-intensity–versus–depth curve, λ. Basic to this derivation

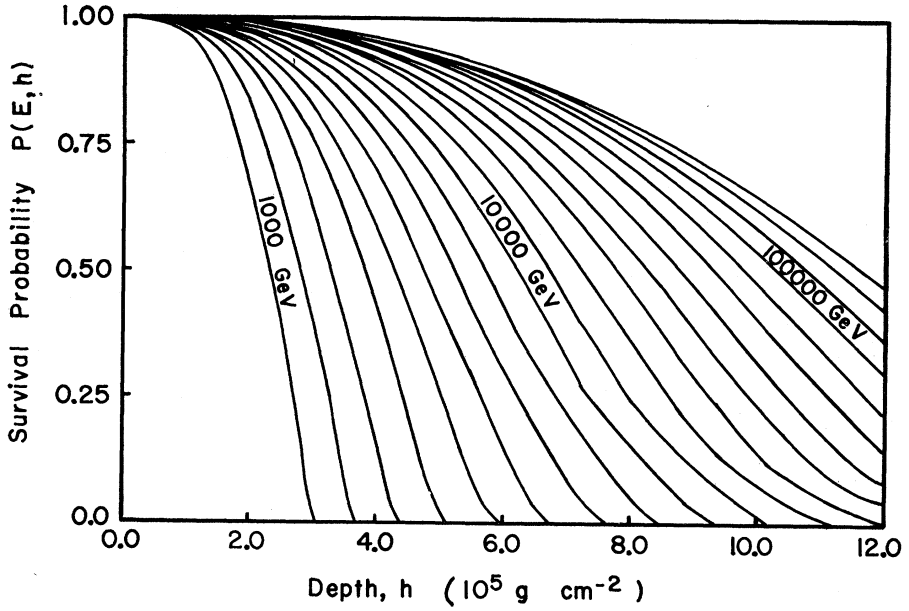

FIG. 15. Survival probability versus depth for muons in standard rock. The energies are a parameter and belong to a geometric sequence. Photonuclear cross section $=0.72\times10^{-28}$ cm^2.

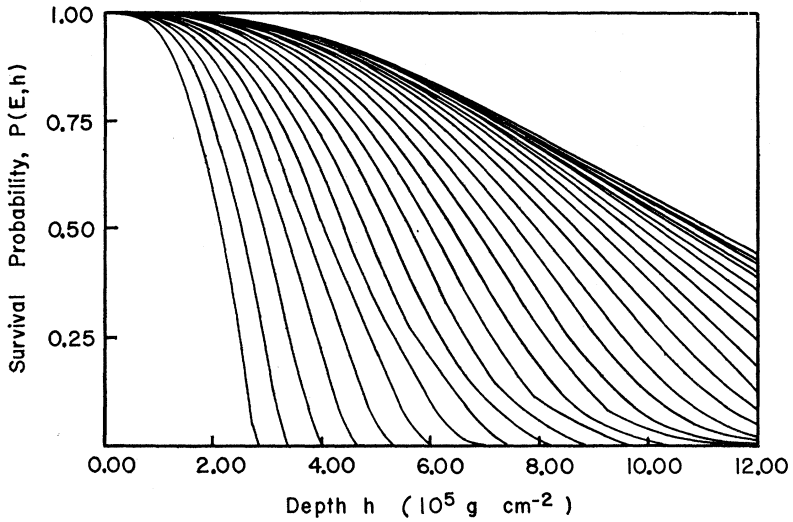

FIG. 16. Survival probability versus depth for muons in standard rock. The energies are a parameter and belong to a geometric sequence. Photonuclear cross section $=3.6\times10^{-28}$ cm^2.

are the energy-loss formulas for muons given in Appendix B. The average energy-loss coefficient b for standard rock is calculated to be $(4.35\pm0.30)\times10^{-6}$ cm^2 g^{-1} when the photonuclear cross section is 0.72×10^{-28} cm^2. The error in b represents our uncertainty in the theoretical energy-loss mechanisms of pair production and bremsstrahlung.

Following the established practice,[18] we assume a power law for the energy spectrum of the muons in the atmosphere, i.e., that $N(E)dE$, the number of muons with energy between E and $E+dE$, is

$$N(E)dE=\gamma AE^{-\gamma-1}dE. \tag{16}$$

Then $I(h)$, the intensity of muons at the depth h underground, is

$$I(h)=\int_0^\infty \gamma AE^{-\gamma-1}P(E,h)dE. \tag{17}$$

The ratio of intensities at two depths h_1 and h_2 given by Eq. (17) can be combined with Eq. (2) to relate γ and λ:

$$\frac{h_2-h_1}{\lambda}=\ln\left[\frac{I(h_1)}{I(h_2)}\right]. \tag{18}$$

1. secθ *Angular Distribution for Muons in the Atmosphere*

Figure 17 shows γ versus λ for various values of the photonuclear cross section. Using the experimental

[18] P. H. Barrett, L. M. Bollinger, G. Cocconi, Y. Eisenberg, and K. Greisen, Rev. Mod. Phys. 24, 133 (1952).

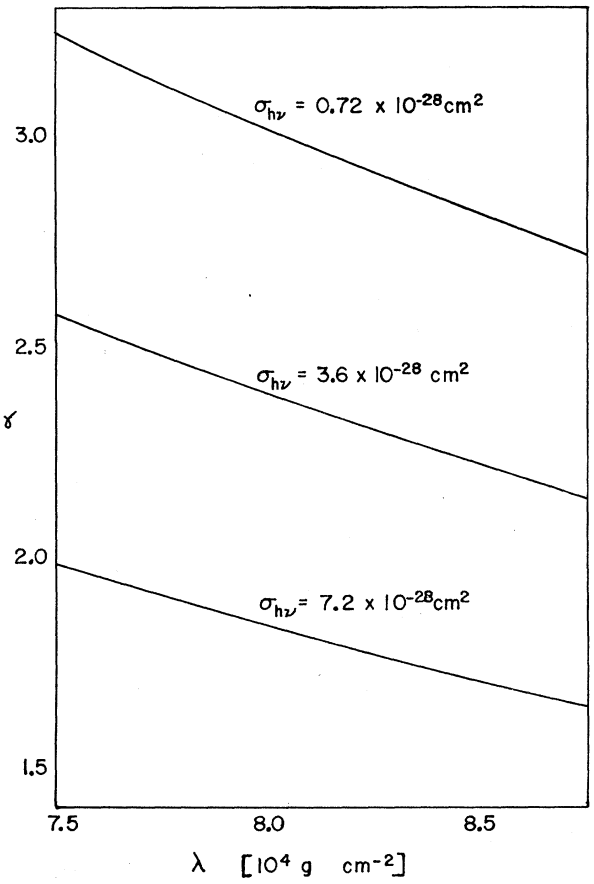

FIG. 17. Relationship between λ and the spectral index γ for various values of the photonuclear cross section.

value $\lambda=(8.04_{-0.39}{}^{+0.35})\times10^4$ g cm^{-2} (Table V) and $b=(4.35\pm0.44)\times10^{-6}$ cm^2 g^{-1}, we find that $\gamma=2.99\pm0.35$. Here, we have estimated the error in b to be $\pm10\%$ and have used a photonuclear cross section of 0.72×10^{-28} cm^2. We have used the experimental depth-intensity curve at an arbitrary depth and Eq. (17) and have found the parameter A to be 8.5×10^1 cm^{-2} sec^{-1} sr^{-1} for $\gamma=2.99$.

Using data from many sources, mainly from extensive air showers, Vernov and Khristiansen[19] have found the energy spectrum of the primary cosmic rays. Their results show that it is a power law with spectral index -1.6 ± 0.1 for energies up to 3×10^{15} eV. If we assume this value for the primaries and further assume that the muons in the atmosphere are produced by the decay of π and K mesons, then, at energies large compared with 10^{11} eV,[20] such muons will have a spectral index of -2.6 and will have an angular distribution in the atmosphere which is enhanced by a factor secθ. Although the experimentally determined spectral index for the secθ angular distribution is not inconsistent with this prediction, in order to get exact agreement it would be necessary to increase b to 5.10×10^{-6} cm^2 g^{-1}.

2. *X-Process Contribution to Muon Production*

Keuffel's group at the University of Utah[2,15,21] have measured the intensity of cosmic-ray muons underground as a function of depth and zenith angle. A comparison of their data with the depth-intensity curve available to them showed a departure from the approximate secθ enhancement expected if the muons were produced by the decay of pions and kaons in the atmosphere.[15] This departure led the Utah group to postulate[21] a new production mechanism for muons. This so-called X process yields muons either directly or by means of a sufficiently short-lived intermediary. The spectrum of muons produced in this manner would have an index identical with that of the primary radiation and an isotropic angular distribution in the atmosphere. The cross section for the X process required by their data was estimated by the Utah workers to be a few percent of the π, K mechanisms.

It is of interest to reexamine the Utah data in the light of the Case-Wits-Irvine (CWI) vertical-depth-intensity curve. To do this, we must convert the Utah depths to standard rock using Eqs. (11) and (B7). The density correction noted by Keuffel *et al.*[22] has also been made.

If there were 100% X process for energies greater than or equal to that corresponding to 4×10^5 g cm^{-2}, the Utah data would fall on the vertical-intensity curve which we derived assuming an isotropic distribution in the atmosphere.

If the X process did not exist, the Utah data would show an enhancement over the vertical-intensity curve of approximately secθ.

According to the model of Bergeson *et al.*,[21] the muons are produced partly by the decay of π and K mesons, and partly by the X process. Using the energy-dependent relative probability for X process as given by these authors, we predict an enhanced intensity which lies closer to the secθ curve at low energies and which slowly approaches the isotropic curve as the energy (or depth) increases. This is illustrated in Figs. 18 and 19. The experimental points of the Utah group are not inconsistent with this derived curve. We therefore conclude that the CWI vertical-intensity-depth relationship does not exclude an X process of the magnitude proposed by the Utah group.

If the X process does exist, the muons observed underground should have an energy-dependent spectral index which is intermediate to the $\gamma=-2.6$ due to π and K decay and the $\gamma=-1.6$ of a direct production

[19] S. N. Vernov and G. B. Khristiansen, in Proceedings of the Tenth International Cosmic Rays Conference, Calgary, Canada, 1967, p. 345 (unpublished).

[20] The energy required to penetrate 4×10^5 g cm^{-2} of rock is in excess of 10^{12} eV.

[21] H. E. Bergeson, J. W. Keuffel, M. O. Larson, G. W. Mason, and J. L. Osborne, Phys. Rev. Letters **21**, 1089 (1968).

[22] J. W. Keuffel, Utah Acad. Sci. Proc. **45**, 1 (1968).

process. Bergeson *et al.* have assumed that the photonuclear cross section is much larger at these energies than previously expected. From Fig. 17, we note that if we use the measured slope of the depth-intensity curve, $\lambda=8.08\times10^4$ g cm^{-2}, an increase in the energy-loss coefficient is indeed indicated.

IX. SUMMARY

We have observed cosmic-ray muons at a depth of 8.71×10^5 g cm^{-2}. The measured rate has been used together with the data of other workers at shallower depths to determine a new and more accurate depth-intensity curve for depths greater than 4×10^5 g cm^{-2}. The calculated intensities are given in Table VI, the derived parameters for the depth-intensity curve are given in Table V. For a secθ angular distribution of cosmic-ray muons in the atmosphere and a $(1-0.67\cos^2\theta)$ distribution for neutrino-induced muons, the derived depth-intensity relationship $I(h)=a_\mu e^{-h/\lambda}$ has parameters $a_\mu=(1.04_{-0.13}{}^{+0.21})\times10^{-6}$ cm^{-2} sec^{-1} sr^{-1} and $\lambda=(8.04_{-0.39}{}^{+0.35})\times10^4$ g cm^{-2}. A previous determination of these parameters by Menon *et al.*,[12] using preliminary results from the present experiment, gave $a_\mu=9.8\times10^{-7}$ cm^{-2} sec^{-1} sr^{-1} and $\lambda=(8.10\pm0.50)\times10^4$ g cm^{-2}.

An improved numerical method for calculating the fluctuations in the ranges of muons in rock has been developed, and the technique has been used to relate the spectral index of the atmospheric muons to the slope of the intensity-versus-depth curve. For the secθ and $(1-0.67\cos^2\theta)$ distributions, the spectral index so derived is 2.99 ± 0.35. The corresponding number derived from extensive air showers is 2.6 ± 0.1. Better agreement with the air-shower result can be achieved by increasing the energy-loss coefficient b by about 17%, though we appreciate the possibility that the difference in the two numbers may, in fact, be due to statistical fluctuations.[23] One way of improving the agreement would be to increase the photonuclear cross section by a factor of 3.5.

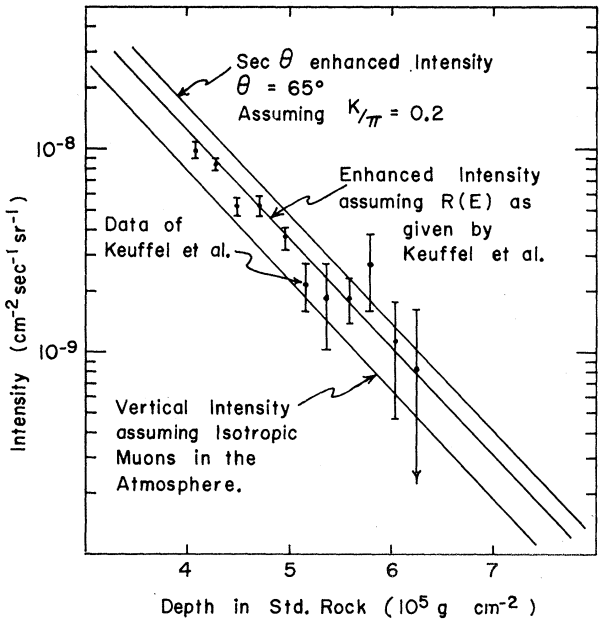

FIG. 18. Comparison of the vertical intensity with intensities measured at inclined angles. Here $\theta=60°$–$70°$.

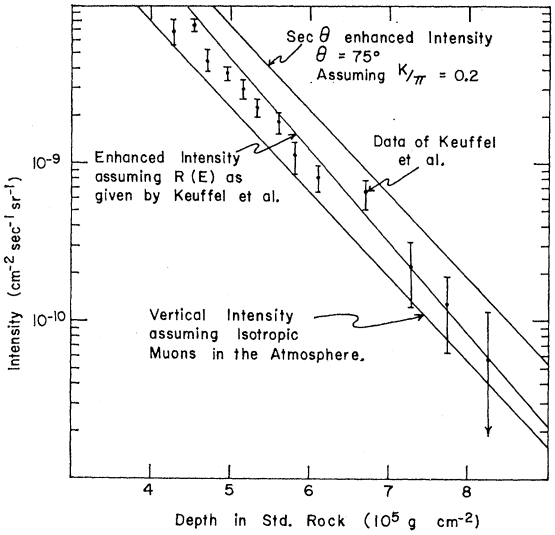

FIG. 19. Comparison of the vertical intensity with the intensities measured at inclined angles. Here $\theta=70°$–$80°$.

ACKNOWLEDGMENTS

We wish to thank Dr. T. L. Jenkins and B. M. Shoffner for their help in the early phases of this work. R. Atkinson and J. Baird helped maintain and operate the equipment. G. Nelson and M. Stein read and assisted in the interpretation of our film records. The assistance and cooperative attitude of the men of the East Rand Proprietary Mines is gratefully noted. A special word of appreciation is due our engineer, A. A. Hruschka, for his vital part in the design, construction, and installation of the detector deep underground.

APPENDIX A: APERTURES OF ARRAY

A computer program was written to evaluate the aperture as a function of zenith angle for each of the seven event categories. This calculation supplemented the analytic calculation of the total apertures made earlier. The sensitive area of the detector array for each direction was found by projecting the array onto a vertical plane parallel to and alongside a face of the array. The areas belonging to the various categories were found by considering the different regions of over-

[23] It is recognized that absorption methods such as those used here are difficult to interpret, and an attempt is underway at the University of California, Irvine, to measure the muon interaction cross sections directly, using an appropriate spectrometer and target detector array located at the earth's surface.

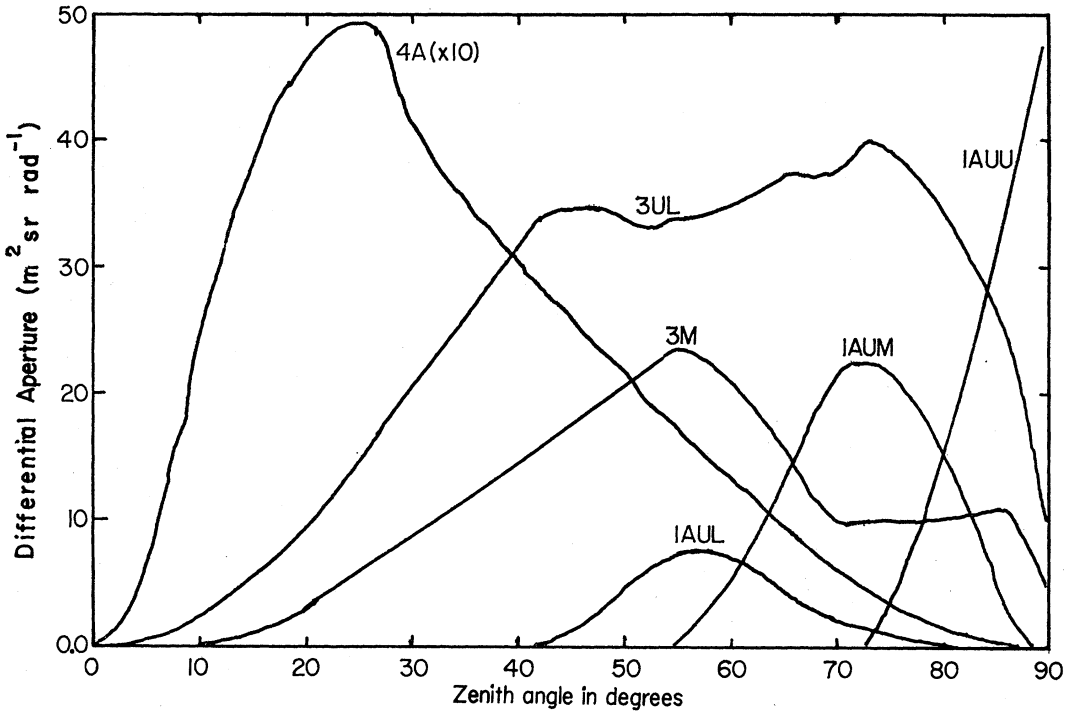

FIG. 20. Differential apertures versus zenith angle for single muons in bays 1–6.

lap between the projections of the tanks. Each of these areas was then multiplied by the differential $\sin\theta\, d\varphi$ and the cosine of the angle between the normal to the projection plane and the chosen direction in space. These were summed over the azimuthal angle φ to give the differential aperture $dA/d\theta$.

The program considered two projections of each element: one representing the region of the element in

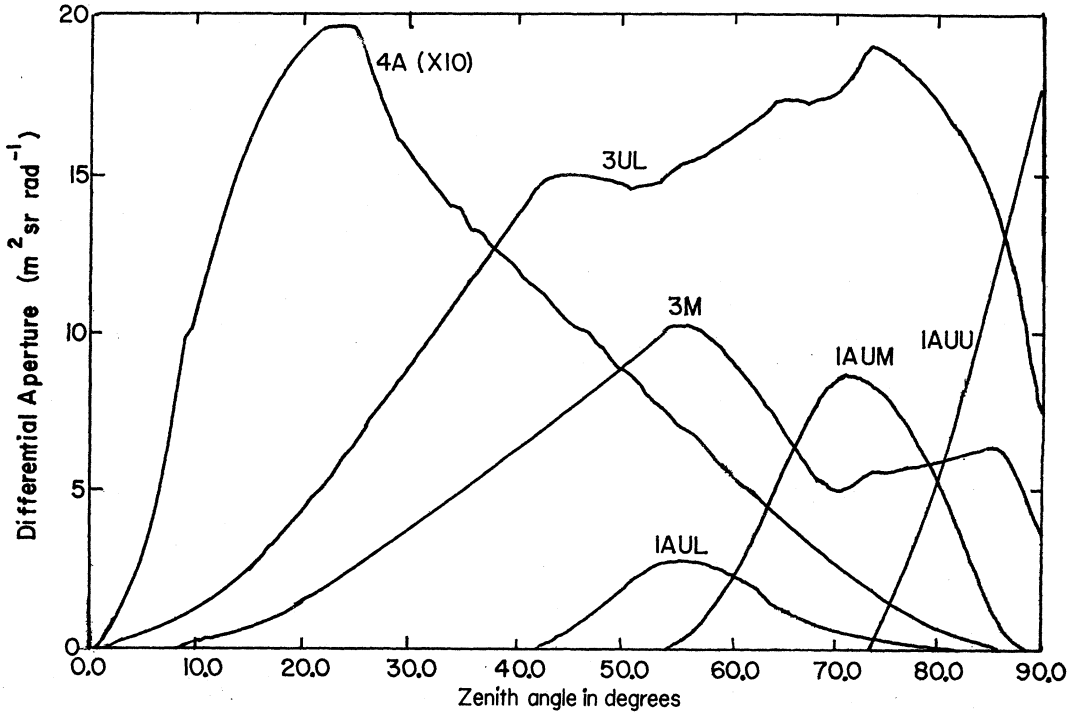

FIG. 21. Differential apertures versus zenith angle for single muons in bays 7–9.

TABLE X. Total apertures of the detector array for isotropic radiation. A minimum path length corresponding to an 18-MeV threshold has been incorporated into the calculation.

Type of event	Class	Bays 1–6 (m^2 sr)	Bays 7–9 (m^2 sr)	Summed over sr
1A	UU	50.1	18.9	4π
1A	UM	58.2	21.8	4π
1A	UL	20.0	7.3	4π
3	UL	149.0	69.6	2π
3	M	65.4	31.1	2π
4A		12.8	5.3	2π
4B		1.6	0.84	2π

which a muon would cause signals large enough for triggering and one representing the region in which a muon would give rise to signals large enough to be seen on the photographic oscilloscope records.

Table II gives the dimensions of the array. Figures 20 and 21 show the differential apertures calculated in this way for the two parts of the system. Table X gives the total apertures of the array ($dA/d\theta$ integrated over θ) for the various event categories. These totals illustrate the large size of the array, but their use is limited to isotropic radiation.

APPENDIX B: INTERACTIONS OF HIGH-ENERGY MUONS

The processes through which muons interact with matter can be divided into two types: continuous and catastrophic. In the first, the muon makes frequent encounters with atoms losing in each a very small fraction of its energy. For any finite thickness of matter the number of such encounters is large and proportional to the thickness traversed. Ionization is an example of a continuous process. In the second type of interaction, the muon loses a large but random fraction of its energy. Bremsstrahlung is an example of a catastrophic process.

The processes of ionization and excitation of atoms, and the production of knock-on electrons, are considered here as continuous. The energy-loss formulas for these processes combine to give the well-known formula[24]

$$-\frac{dE}{dh}=\frac{2\pi ne^4Z^2}{mv^2\rho}\left[\ln\frac{m^2c^2E}{2\pi\hbar ne^2}-\frac{3}{4}\right]. \quad \text{(B1)}$$

In this equation, E is the muon energy, e the electronic charge, m the electron mass, c the velocity of light, and $\hbar$ is Planck's constant divided by 2π. Z is the average atomic number of the rock atoms, ρ is the rock density, n its electron density, and h the thickness of rock (in g cm^{-2}).

The catastrophic processes are expressed by giving the probability per unit thickness of matter that the muon will lose a fraction between V and $V+dV$ of its energy. The catastrophic loss due to bremsstrahlung[25] for muon energies $>10^{11}$ eV is given by

$$\phi_B(V)dV=0.95\alpha(N/A)(2rm/\mu)^2 \times Z(Z+1.3)(\tfrac{4}{3}+V^2-\tfrac{4}{3}V)(dV/V) \times\ln\left(\frac{\frac{3}{2}K(\mu/m)Z^{-2/3}}{\frac{1}{2}Ke^{1/2}(\mu^2/mE_0)[V/(1-V)]Z^{-1/3}+1}\right). \quad \text{(B2)}$$

Here, N is Avogadro's number, μ is the mass of muon, E_0 is the initial muon energy, α is the fine-structure constant, r is the classical electron radius, and $K\simeq 190$.

The production of electron-positron pairs requires a slightly more complex formula[26] since the electron and the positron may share the energy lost by the muon in any proportion. We define $U=(\epsilon_+-\epsilon_-)/(\epsilon_++\epsilon_-)$ and $\epsilon=\epsilon_++\epsilon_-$, where ϵ_+ is the energy received by the positron and ϵ_- is the energy received by the electron.

We have[27]

$$\phi(E,V,U)dUdV=(2N/\pi A)0.95Z(Z+1.3)(r\alpha)^2 \times[(1-V)/V](\phi_a+\phi_b)dUdV, \quad \text{(B3)}$$

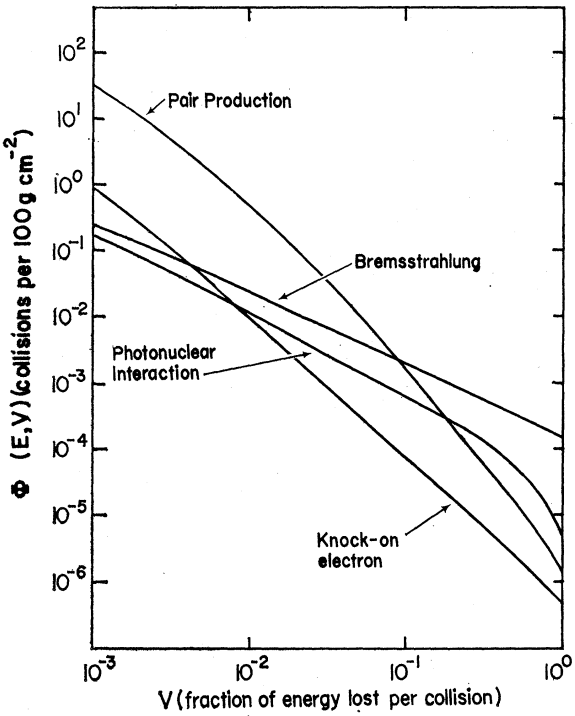

FIG. 22. A comparison of the catastrophic energy-loss mechanisms for 10-TeV muons in standard rock.

[24] R. M. Sternheimer, in *Methods of Experimental Physics*, edited by L. C. L. Yuan and C. S. Wu (Academic, New York, 1961), Vol. 5, Part A, p. 1.

[25] I. L. Rosenthal', Usp. Fiz. Nauk 94, 91 (1968) [Soviet Phys. Usp. 11, 49 (1968)].

[26] S. R. Kel'ner, Yadern. Fiz. 5, 1092 (1967) [Soviet J. Nucl. Phys. 5, 778 (1967)].

[27] We note in Ref. 25 an error in the formula for the cross section for direct pair production. In formula (1.11) of this reference the ratio of the muon energy after and before collision appears inverted.

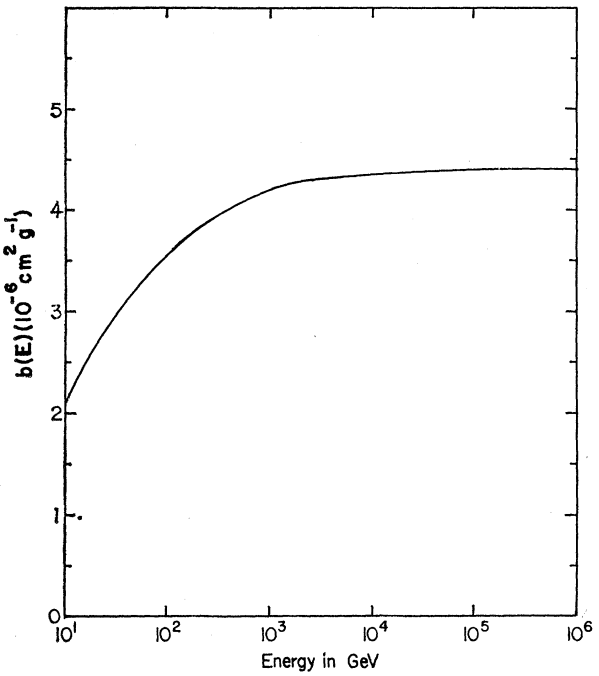

FIG. 23. Coefficient of the average energy loss due to catastrophic processes for muons in ERPM rock for $\sigma_{h\nu}=0.72\times10^{-28}$ cm².

where ϕ_a and ϕ_b are derived by Kel'ner[26] for both screening and no-screening conditions. Choice between screening and no screening is made according to the value of the parameter

$$\xi=\frac{1}{2\alpha Z^{1/3}}\frac{V}{1-V}\frac{\mu}{m}\frac{\mu c^2}{E}. \tag{B4}$$

If $\xi<1$, we use the screening formulas and if $\xi>1$, we use the no-screening case.

In order to evaluate $\phi_p(E,V)dV$, the probability per unit thickness that the muon loses a fraction between V and $V+dV$ of its energy, Eq. (B3) must be integrated over U.

The third catastrophic process is the photonuclear interaction. We use the form given by Kobayakawa,[28]

$$\phi_N(E,V)dV=\frac{\alpha N\sigma_{h\nu}}{2\pi}\frac{dV}{V}\left\{0.9\left[2-2V+\left(1+\frac{4}{\lambda_1}\right)V^2\right]\times\left[\left(1+\frac{3}{2\lambda_1}\right)\ln\lambda_1-1+\ln\left(\frac{1-V}{V^2}\right)\right]-2(1-V)+0.1[1+(1-V)^2]\times\ln\left(\frac{2ME(1-V)}{\mu^2c^2V}\right)\right\}, \tag{B5}$$

where $\sigma_{h\nu}$ is the photonuclear cross section which, though generally assumed to be constant, may very well be a function of energy; $\lambda_1=32.69$; and M is the nuclear mass.

The accuracy of the bremsstrahlung and pair production cross sections is estimated to be $\sim5\%$.[25] The photonuclear interaction is not well known, and Kobayakawa estimates that the cross section is only good to $\sim30\%$.

Figure 22 is a comparison of the probabilities $\varphi(E,V)$ due to the three catastrophic processes described above and that due to knock-on electrons, for 10-TeV muons in standard rock. It is clear from this figure that the contribution of the knock-on process is small compared with the other three processes. This is the justification for including it with the continuous processes.

A quantity of interest is the average rate of energy loss due to the catastrophic processes. Adding the probabilities for bremsstrahlung, pair production, and photonuclear interaction, we obtain $\Phi(E,V)dV$, the probability per unit thickness that a muon of energy E loses a fraction between V and $V+dV$ of its energy. Multiplying by VE and integrating over V, we get

$$-\frac{dE}{dX}=E\int_0^1 V\Phi(E,V)dV=b(E)E. \tag{B6}$$

Equation (B6) defines the energy-loss coefficient b. The variation of b with energy is shown in Fig. 23. It can be seen from this figure that for energies greater than ~10 TeV, b is constant if the photonuclear cross section is constant. For these energies, Eq. (B6) leads to the relationship

$$b=7.34\times10^{-7}(Z^2/A)+4.26\times10^{21}\sigma_{h\nu}. \tag{B7}$$

[28] K. Kobayakawa, Nuovo Cimento 47B, 156 (1967).